AJP

ISSN : 0971 - 3093

Vol 24, No 12, December, 2015

ASIAN JOURNAL OF PHYSICS

An International Quarterly Research Journal

ANITA PUBLICATIONS

FF-43, 1st Floor, Mangal Bazar, Laxmi Nagar, Delhi-110 092, India

B O : 2, Pasha Court, Williamsville, New York-14221-1776, USA

ap

Available on www.asianjournalofphysics.in
Invited Article

Asian Journal of Physics Vol. 24, No 12 (2015) 1667-1677

Coherence-based 3D and spectral imaging

Masaki Obara[1], Kyu Yoshimori[1] and Kazuyoshi Itoh[2]

[1]*Department of Electrical Engineering and Computer Science, Graduate School of Engineering, Iwate University, 4-3-5, Ueda, Morioka, Iwate, 020-8551, Japan*

[2]*Science Technology Entrepreneurship Laboratory (E-Square), Osaka University, 2-1, Yamada-oka, Suita, Osaka, 565-0871, Japan*

Dedicated to Prof Joseph Shamir

The multi-spectral three-dimensional (3D) imaging has been demanded in a variety of fields. In the interferometric measurement, a set of spectral components of 3D images, that is, multi-spectral 3D images can be retrieved from the 3D spatial coherence function that describes the spatial correlation of the light. The authors explain the principle of the Fourier-transform spectral imaging technique and an overview of the method for measurement of spatial coherence function. Furthermore, authors report the recent progress in the fields associated with this technique.

Keywords: Fourier-transform, Holography, Spatio-spectral image, Fourier-transform, Radio astronomy

1 Introduction

In 1921, Albert A Michelson succeeded in measuring the diameter of the super-giant star Betelgeuse at the Mount Wilson Observatory with his coworkers [1]. He used a 6-meter periscope-type interferometer on the front of the 2.5-meter telescope. The principle of image reconstruction using his famous interferometer, the Michelson stellar interferometer, is the same as that of the incoherent holography [2]; the Van Cittert-Zernike (VCZ) Theorem [3]. The radio interferometers working worldwide are also resting on the same principle [4]. Michelson on the other hand studied the spectral shape of a light source using his another famous interferometer; Michelson interferometer or Michelson-Morley interferometer [5] by detecting the dynamic fringes formed by interference between light beams with an increasing time delay. This is the origin of the Fourier spectrometers today. Both of the interferometers that are brought into existence by Michelson are still now playing important roles in the world today.

If you properly combine these interferometers, you can reconstruct a spatio-spectral image, which is a two-dimensional (2D) array of spectra at each location over the object surface. The principle is based on a Fourier-transform relationship derived from the basic propagation formula describing the field correlation function in terms of the source correlation function [6] and can be considered as a unification of the VCZ and Wiener-Khinchine theorems. The theory was published in 1986 with a simple experiment [7]. Shortly after, Mariotti and Ridgway suggested a simple and quite effective combination of these interferometers for use in astronomy [8]. The Long-baseline ground-based type of this spatio-spectral interferometers using optical single-mode fibers [9,10] and a similar type of ground-based system without the use of single-mode fibers [11,12] are under study. In the field of radio astronomy, spatio-spectral imaging is relatively easy, because the radio wave is directly detectable by an antenna and the time delay for the correlation can readily be introduced electronically. The temporal correlation function or the coherence function for each base line is usually measured first by an analogue or digital correlator depending on the generations [13-15] and the cross-power or cross-correlation functions is calculated by the Fourier transform relationship [4,16]. The detected wavelength ranges for example from 6 to 50 cm [15] and 0.8 to 30 cm [17]. Chikada *et al* constructed a

Corresponding author :
e-mail: masaki@ql.cis.iwate-u.ac.jp (Masaki Obara)

modern FFT spectrum analyzer with the highly parallel pipeline architecture where the digitized radio signals are numerically Fourier transformed before the correlation process [18].

Several projects of space-borne optical or infrared interferometers are also in progress [19-21]. The SPIRIT [19] will have the high angular resolution (0.3 arcsec) and the detection wavelength ranges from 25 to 400 μm. For details readers are referred to Ref [19]. The authors believe that the space-borne optical interferometers are the most promising application of the Fourier-transform spectral imaging or double Fourier technique.

To record a hologram for incoherently illuminated or self-luminous object, many techniques have been investigated. The light emitted from each point on the spatially incoherent object interferes only with itself. The recorded hologram is explained as the incoherent superposition of Fresnel zone patterns from each point on object. From the nature of light, in the branch of optics concerned with incoherent holography, we may find a variety of ideas. Marks *et al* report that it is possible to obtain fully 3D images of spatially incoherent objects by combining cone-beam tomography schemes and interferometric measurement from a rotational shear interferometer [22]. Additionally, the method that is based on the interferometry and phase shifting by diffractive optical element displayed on the spatial light modulator, called Fresnel incoherent correlation holography (FINCH), has been proposed by Rosen *et al*. The FINCH was demonstrated for mercury arc lamp illumination of objects [23] and for 3D fluorescent objects [24]. Besides, several attractive incoherent holographic techniques have been proposed recently such as color holographic recording under natural daylight illumination [25], measurement of the spatial and temporal correlation function using Mach-Zehnder interferometer [26].

In this paper, the authors explain the principle of the Fourier-transform spectral imaging technique as simply as possible and then introduce briefly the current status of the Fourier-transform spectral imaging technique for astronomy and then the novel interferometric, 3D and spectral imaging technique that may be applied to imaging applications for multi-spectral fluorescent particles in biological fields.

2 Coherence-based spectral imaging technique

The spectral imaging technique to be discussed here is, as already mentioned, based on the unified theory combining the principles of the Michelson's two well-known interferometers. The unified theory states that if you can measure the 3D spatial coherence function of optical disturbances coming from the far zone you can retrieve at one sweep both of the spatial and spectral information of the light source. The principle will be explained in an intuitive and comprehensible way using a simple light source model.

2.1 Principle of the Fourier-transform spectral imaging

Let us consider the 3D spatial coherence of optical field illuminated by a simple object in the far zone. Here we assume two point sources as shown in Fig 1. The point sources in the $z = 0$ plane emit mutually incoherent quasi-monochromatic lights. Here, "incoherent" means the lights from the two point sources are statistically independent and "quasi-monochromatic" means that the spectral width of the light is very small compared with the average frequency. For simplicity we assume that the observation area is located sufficiently far from the light sources and the optical waves coming from the two light sources can be considered to have flat or planar wavefronts. We also assume to focus on a certain component of polarization and deal with the optical field as scalar.

Let the two point sources be numbered ($j = 1,2$) and the mean 3D wavenumber vectors and mean angular frequencies be $\bar{\boldsymbol{k}}_j$ and $\bar{\omega}_j = c\bar{k}_j$, respectively. Then, the optical wave field at the location $\boldsymbol{R}$ in the observation area at time t is given by

$$V(\boldsymbol{R},t) = V_1(\bar{\boldsymbol{k}}_1 \cdot \boldsymbol{R} - \bar{\omega}_1 t)\exp[i(\bar{\boldsymbol{k}}_1 \cdot \boldsymbol{R} - \bar{\omega}_1 t)] + V_2(\bar{\boldsymbol{k}}_2 \cdot \boldsymbol{R} - \bar{\omega}_2 t)\exp[i(\bar{\boldsymbol{k}}_2 \cdot \boldsymbol{R} - \bar{\omega}_2 t)], \quad (1)$$

where $V_j(\bar{\boldsymbol{k}}_j \cdot \boldsymbol{R} - \bar{\omega}_j t)$ means a slowly-varying envelope function that changes very slowly compared with the mean frequency or mean wavelength. The real parts of these envelope functions are drawn in Fig. 1 by the thick lines. It is important to note that the shape or statistics of this envelope function depends on the light source and statistically random in nature. As a constant quantity that can be uniquely defined, we have

$$\Gamma(\boldsymbol{R}_1, \boldsymbol{R}_2; \tau) \equiv \langle V^*(\boldsymbol{R}_1, t) V(\boldsymbol{R}_2, t+\tau) \rangle , \tag{2}$$

where * denotes the complex conjugate, ⟨K⟩ means the statistical ensemble average, and the temporal stationarity of the optical field is assumed and the ensemble average can usually be considered to be replaceable with the time average.

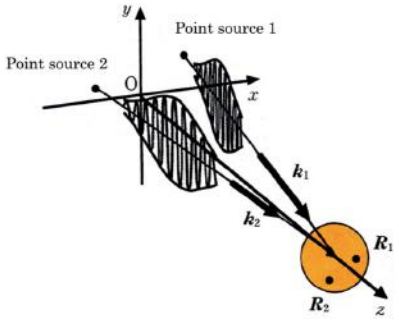

Fig 1. Optical field generated by the two point sources in the far zone.

It is important to note that the two point sources are statistically independent, and the lights coming from the two light sources do not interfere or do not form stable fringes. In other words, they are always mutually generating an ensemble of time-varying beats. Thus, $V_1(\bar{\boldsymbol{k}}_1 \cdot \boldsymbol{R} - \bar{\omega}_1 t)$ and $V_2(\bar{\boldsymbol{k}}_2 \cdot \boldsymbol{R} - \bar{\omega}_2 t)$ have no statistical correlation that is $\langle V_1^*(\bar{\boldsymbol{k}}_1 \cdot \boldsymbol{R} - \bar{\omega}_1 t) V_2(\bar{\boldsymbol{k}}_2 \cdot \boldsymbol{R} - \bar{\omega}_2 t) \rangle = 0$. Then, from Eqs (1) and (2) we have

$$J(\boldsymbol{R}_1, \boldsymbol{R}_2) \equiv \Gamma(\boldsymbol{R}_1, \boldsymbol{R}_2; 0) = \langle |V_1|^2 \rangle \exp[i\bar{\boldsymbol{k}}_1 \cdot (\boldsymbol{R}_2 - \boldsymbol{R}_1)] + \langle |V_2|^2 \rangle \exp[i\bar{\boldsymbol{k}}_2 \cdot (\boldsymbol{R}_2 - \boldsymbol{R}_1)] . \tag{3}$$

From Eq (3), we understand that the two mutually independent point sources produce coherence function in the far field and it depends only on the relative positions $(\boldsymbol{R}_2 - \boldsymbol{R}_1)$ and produce a pair of uniform complex fringes . This is the typical coherence function produced by the fixed stars in the night sky in front of our eyes. The period and direction of the complex fringe is determined by each 3D wave vector, $\boldsymbol{k}_j$ the amplitude of the fringe is proportional to the brightness of the point source. It is now clear that if we take the Fourier transform of Eq (3), we get in the wave vector space the delta-like functions located at $\bar{\boldsymbol{k}}_1$ with strength proportional to $\langle |V_j|^2 \rangle$. Every luminous objects or objects illuminated by substantially incoherent light can be considered as a collection of mutually independent light sources, the above discussion directly applies to general extended incoherent objects.

The principle of spectral imaging has been explained by using a simple light source model. But for general discussions, the propagation of cross-spectral density is adequate. Itoh and Ohtsuka [7] derived a general formula resting on the work by Carter and Wolf [6] as

$$J(\boldsymbol{R}_1, \boldsymbol{R}_2) \equiv \int d\omega d^2 r_\perp S_\omega(\boldsymbol{r}_{s\perp}, 0) \frac{\exp[i\bar{\boldsymbol{k}} \cdot (|\boldsymbol{R}_2 - \boldsymbol{r}_\perp| - |\boldsymbol{R}_1 - \boldsymbol{r}_\perp|)]}{|\boldsymbol{R}_1 - \boldsymbol{r}_\perp||\boldsymbol{R}_2 - \boldsymbol{r}_\perp|} , \tag{4}$$

where $S_\omega(\boldsymbol{r}_{s\perp}, 0)$ is the spectral intensity distribution of the incoherent light source in the 2D object plane at a point $\boldsymbol{r}_{s\perp}$. Equation (4) includes both of the spatial and spectral information of object and can be considered as the extension of the VCZ theorem to polychromatic objects.

They derived under appropriate conditions the following equation:

$$J(\boldsymbol{\rho}) = \int d^3k G(\boldsymbol{k}) \exp(i\boldsymbol{k}.\boldsymbol{\rho}), \tag{5}$$

where

$$J(\boldsymbol{\rho}) = J(R,\ R+\boldsymbol{\rho}), \quad G(\boldsymbol{k}) = c(kk_z)^{-1} S_\omega(\boldsymbol{r}_{s\perp}(\boldsymbol{k}),0). \tag{6}$$

They showed that from the Fourier inversion relationship the function $G(\boldsymbol{k})$ can be retrieved from the coherence function in the observation area, $J(\boldsymbol{\rho})$ and named the function $G(\boldsymbol{k})$, the spectral image.

If the object has no spatial variations and you don't care about the inner structure, you may measure the coherence function like $J(\boldsymbol{\rho}) = J(0,0,\Delta z)$, and you get only the spectral information without the spatial information via one-dimensional Fourier transformation. If the object is monochromatic and you don't care about the spectral information, you may measure the coherence function like $J(\boldsymbol{\rho}) = J(\Delta x, \Delta y, 0)$, and you get the spatial intensity distribution of object without the spectral information. Thus, Eq (5) is said to unify the VCZ and Wiener-Khinchine theorems. Resting on Eq (5), you can estimate for example the signal deteriorations due to the finite extent of detection aperture in Fourier spectrometry and/or image degradations due to the fact that the base lines in the earth rotation aperture synthesis are not in a single plane [27].

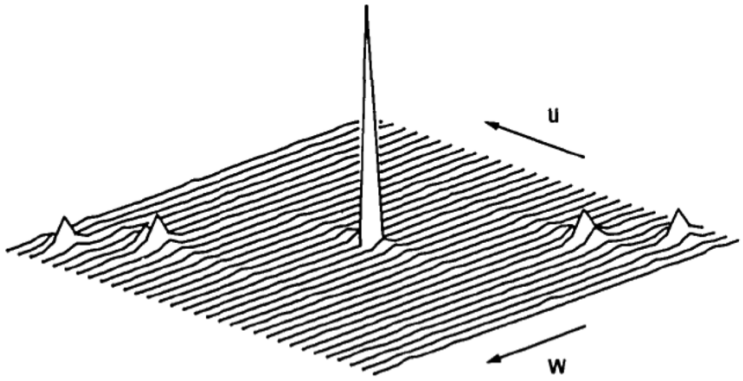

Fig 2. Reconstructed spectral image of a point object composed of He-Cd (4416-A) and He-Ne (6328-A) laser spectra.

Figure 2 shows the 2D spectral image reconstructed experimentally [27]. A point object with two spectral components was produced by focusing a light beam composed of He-Cd (4416-A) and He-Ne (6328-A) laser spectra. The coordinates (u,w) correspond to (ρ_x, ρ_z) in this paper, respectively. You can see the two spectral components lie on the same radial line, which indicates the angular position of object. The authors also discussed briefly on the signal to the noise ratio for astronomical observation of stars.

2.2 Space interferometer

The Herschel and Hubble Space Telescopes achieved great success because of the absence of the surrounding atmosphere, but the astronomers at any time require the resolution as high as possible. The double-Fourier spatio-spectral technique is suggested assuming aperture synthesis for the very high spatial resolution [8]. The concept of the double Fourier interferometer is shown in Fig 3 [8,27]. As can be seen, the interferometer is a simple combination of the two famous interferometers due to Michelson. The 3D spatial shear is introduced into the incoming optical field and spectral image is retrieved by the principle of the Fourier-transform spectral imaging.

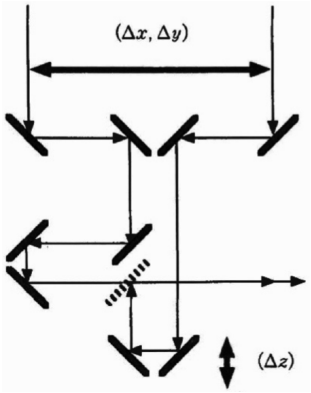

Fig. 3. The concept of the double Fourier interferometer.

Note that the spatial information is maintained by the optical beam in these instruments. Thus, it is possible to retrieve the spatial information from the interference fringes formed in the focal plane as is done in the Wide-field Imaging Interferometry Testbed (WIIT) [20] (to be referred to later). The path-difference introduced into the direction of the optical axis truly introduced to create 3D shear into the field not to create the time shear into the field as is expected in Fourier spectrometry. This is the main difference between the Fourier-transform spectral imaging and the spatio-spectral radio interferometry or long-baseline spatio-spectral optical interferometry using the single-mode optical fibers. The latter ones generate the cross-spectral density by introducing the time delay into the incoming optical fields at two positions with the diffraction limited spatial resolution of the two telescopes or the siderostats.

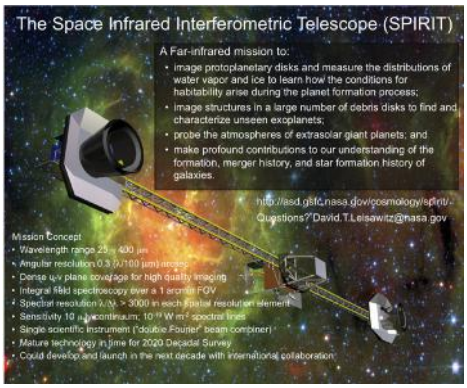

Fig 4. The concept of the Space Infrared Interferometric Telescope (SPIRIT) (Courtesy of David Leisawitz of NASA Goddard Space Flight Center).

The SPIRIT is a space-based spatio-spectral interferometer based on the Fourier-transform spectral imaging or the double-Fourier technique [19]. The aperture synthesis technique [8] provides us much more spatial resolution than the single disc telescope. Figure 4 shows the concept of the Space Infrared Interferometric Telescope (SPIRIT). The SPIRIT is to provide sub-arcsecond resolution images and spectra with resolution R = 3000 in a 1 arcmin field of view in the wavelength range of 25 - 400 μm. The three primary scientific objectives of SPIRIT is as follows: to (1) learn how planetary systems form from protostellar disks, and how they acquire their inhomogeneous composition; (2) characterize the family of extrasolar planetary systems by imaging the structure in debris disks to understand how and where planets of different types form; and

(3) learn how high-redshift galaxies formed and merged to form the present-day population of galaxies. The SPIRIT is to use the wide-field imaging technique employed in WIIT where a detector array was substituted for the usual single detector in the focal plane. Each detector element sees each area in the universe at the given 3D baseline and detects the 3D spatial coherence of incoming light in the parallel fashion. Then, you can get multiple sets of fringe data for wider field of view simultaneously. This simple but very effective technique is to be used in the future interferometers such as SPIRIT and the Balloon Experimental Twin Telescope for Infrared Interferometry (BETTII) [28]. Please note that the SPIRIT is still a pathfinder to the Sub-millimeter Probe of the Evolution of Cosmic Structure (SPECS) [29] and the SPECS is conceived as a 1-kilometer maximum baseline far-IR interferometer requiring multiple spacecrafts flying in a tethered formation.

3 Coherence-based 3D and spectral imaging technique

Interferometric methods to obtain both the 3D spatial information and the spectral information of a usual polychromatic object simultaneously without using coherent illumination, dispersion elements, or image-forming optical elements (such as lenses) have been recently investigated [30-34]. These methods use interferometric techniques and signal processing only. For this purpose, they suggested a method, called digital holographic 3D imaging spectrometry, which are based on measurement of five-dimensional (5D) spatial coherence function and synthetic aperture technique. In this section, we will explain the principle of methods and demonstrate the experimental results to obtain a set of multi-spectral 3D images for spatially incoherent, polychromatic object.

3.1 Principle of the digital holographic 3D imaging spectrometry

A schematic of experiment using the two-wavefront folding interferometer is shown in Fig 5. The measured 3-D object, assumed to be polychromatic and spatially incoherent, is set on the *x*-*y* stage. The wavefront propagated form the object is split by a beam splitter (BS). Each split wavefront is reflected by either the right-angle-prism P or P'. Because the apexes of the two prisms are orthogonal to each other, each split wavefront is reversed, from up to down or right to left, by P or P', respectively. Those wavefronts are superposed again on the BS. The generated fringe pattern, called the elementally interference pattern, is detected by the image sensor. In addition, the lens (L in the figure) projects the surface of the image sensor onto a plane that contains the apex of the prism P'. This plane is regarded as the observation plane. Thus, the object depth (*z*-distance) is measured from this observation plane. To introduce an optical path difference between the two wavefronts, one of the prisms may be displaced along the *z*-axis by the Piezo Translator (PZT). During interferometric measurement, the *x*-*y* stage and PZT are moved stepwise and the relative positions of the two divided wavefronts are changed. Then, 2D elementally interference patterns are recorded at each stage position. In Fig 5, $\hat{x}$ and $\hat{y}$ stand for the *x* and *y* positions, respectively, of the apex of prism P' or P, each of which is being adjusted by movement of the *x*-*y* stage, and *Z* denotes the optical path difference introduced by the PZT. The optical path length between the observation plane and the origin of the Cartesian coordinate system fixed on the *x*-*y* stage is denoted z_0.

Therefore, the 2D elementally interference patterns obtained by the image sensor are arranged three-dimensionally in $(\hat{x}, \hat{y}, Z)$ space. Then, the optical intensity I of the whole data set may be regarded as 5D interferogram, and is expressed using the coordinate system (ξ, η) in the observation plane as

$$I(\xi, \eta, \hat{x}, \hat{y}, Z) = \frac{1}{4}[\Gamma(\boldsymbol{r}, \boldsymbol{r}) + \Gamma(\boldsymbol{r}', \boldsymbol{r}') + \Gamma(\boldsymbol{r}', \boldsymbol{r}) + \Gamma^*(\boldsymbol{r}', \boldsymbol{r})], \tag{7}$$

where * denotes complex conjugate. The 3D position vectors, $\boldsymbol{r} = (\xi + \hat{x}, -\eta + \hat{y}, z_0 + Z)$ and $\boldsymbol{r}' = (-\xi + \hat{x}, \eta + \hat{y}, z_0)$ are the superposed points of the optical fields reflected by prisms P and P', respectively. We suppress the time t in Γ because the optical field is assumed to be stationary in time. In Eq (7), $\Gamma(r,r) = \langle |V(\boldsymbol{r}, t)|^2 \rangle$ and

$\Gamma(\boldsymbol{r}', \boldsymbol{r}') = \langle |V(\boldsymbol{r}', t)|^2 \rangle$ are the optical intensities of the optical field $V(\boldsymbol{r},t)$ at points $\boldsymbol{r}'$ or $\boldsymbol{r}'$, respectively, $\Gamma(\boldsymbol{r}', \boldsymbol{r}) = \langle V^*(\boldsymbol{r}', t)V(\boldsymbol{r}, t) \rangle$ denotes the spatial correlation function of the optical field at points $\boldsymbol{r}$ and $\boldsymbol{r}'$, and the $\langle K \rangle$ stands for the ensemble average.

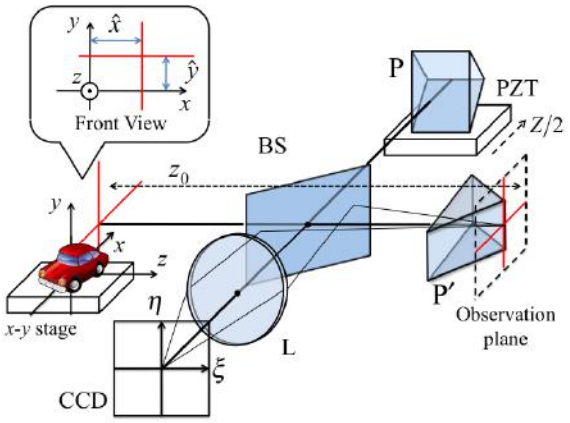

Fig 5. Schematic of two-wavefront folding interferometer.

To compute the reduced volume (3-D) interferogram, we apply the synthetic aperture technique to the 5D interferogram. We will find this interferogram is suitable for retrieving the source information under observation by the selection rule and the rearrangement in new 3D space (X,Y,Z). For generating the volume interferogram, we choose one pixel from each elementally interference pattern according to the selection rule and rearrange the selected pixel. By modifying the selection rule, we may create the various patterns of volume interferogram. One of them is a Spherical-type (S-type) volume interferogram [31,32]. In the S-type volume interferogram, the recorded fringe patterns correspond directly to the phase distributions of the wavefront of many spectral components propagated from the object being measured. Accordingly, the cross-spectral density derived from the S-type volume interferogram corresponds to the ordinary complex hologram. By synthetic aperture technique, the other volume interferograms; Hyperbolic-type (H- type) [33] or Rotated Hyperbolic-type (RH-type) [34] are also generated.

The selection rule for the synthesis of the S-type volume interferogram is written as $(\xi,\eta) = (\hat{x}, -\hat{y})$ {i.e. $\boldsymbol{r} = (\xi + \hat{x}, -\eta + \hat{y}, z_0 + Z) = (2\hat{x}, 2\hat{y}, z_0 + Z)$, $\boldsymbol{r}' = (-\xi + \hat{x}, \eta + \hat{y}, z_0) = (0,0,z_0)$} and the rearrangement rule as $(X,Y) = (2\hat{x}, 2\hat{y})$. The 3D spatial correlation function recorded in the S-type volume interferogram is given by

$$\Gamma(\boldsymbol{R}_0, \boldsymbol{R}_0 + \boldsymbol{\rho}) = c \int_0^\infty dk \exp(ikZ)\, W(\boldsymbol{R}_0, \boldsymbol{R}_0 + \boldsymbol{\rho}_\perp), \tag{8}$$

where

$$W(\boldsymbol{R}_0, \boldsymbol{R}_0 + \boldsymbol{\rho}_\perp) = \int d^3 r_s S_\omega(r_s) \exp\left[i(k_x X + k_y Y)\right] \exp\left(ik \frac{X^2 + Y^2}{2z}\right), \tag{9}$$

is the S-type cross-spectral density at angular frequency $\omega = ck$. Here, $\boldsymbol{R}_0 = (0, 0, z_0)$ denotes the center of the observation plane, the vector $\boldsymbol{\rho} = (X, Y, Z) = (\boldsymbol{\rho}_\perp, Z)$ represents three-dimensional shear from $\boldsymbol{R}_0$. The function $S_\omega(\boldsymbol{r}_s)$ denotes the spectral intensity distribution of 3D object at a point $\boldsymbol{r}_s$, and $z = z_0 - z_s$ is the optical depth of the object, as measured from the observation plane. The example of the computed volume interferogram is shown in Fig 6.

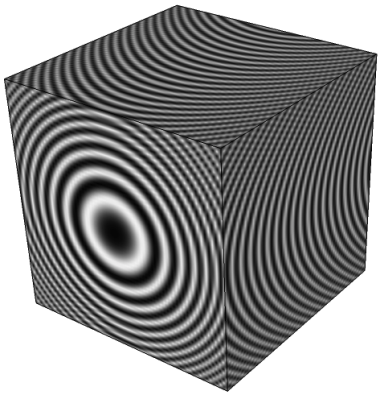

Fig. 6. Example of a theoretical volume interferogram for a monochromatic point source located at the origin of the Cartesian coordinate system.

As we see in Eqs (8), (9), spatial correlation function is expressed as Fourier integral of the cross-spectral density. It is then possible that cross-spectral density may be obtained as Fourier transform of the volume interferogram with respect to Z and taking just the positive frequency part. Since the cross-spectral density in Eq (9) is each spectral component of complex incoherent hologram, a set of spectral components of 3D images can be retrieved from the cross-spectral density by calculating the Fresnel propagation formula.

3.2 Experimental demonstration

We show the experimental results for retrieving the spectral component of 3D image of the light source. The measured object is composed of three planar light sources of each having different continuous spectrum, different shapes, located at different depths. To create three planar light sources of different continuous spectrum, we have attached different color LEDs to the ends of acrylic rods. The cross sections on the other ends of the three rods are shaped as a rectangle and two different triangles. These planar light sources are set up on the *x-y* stage of the two-wavefront folding interferometer. The *x-y* stage of steps and PZT are moved stepwise at constant intervals. The numbers of steps and intervals are 32 and 12.9 μm for the *x-y* stage and 64 and 0.08 μm for PZT, respectively. As a result, the measured 5D interferogram is composed of 32×32×64 elemental interference patterns.

Table. 1 Specification of planar light sources.

Light Source	Peak Wavelength (nm)	Optical depth (mm)	Shape of Planar Light Source
S1	645 (Red)	50	Rectangle
S2	503 (Green)	61	Left-side triangle
S3	450 (Blue)	70	Right-side triangle

The specification of the planar light sources (S1, S2, and S3) is summarized in Table 1. The peak wavelengths of the light sources are 450 nm, 503 nm, and 643 nm. The optical depths of these light sources from the observation plane are 70 mm, 61 mm, and 51 mm, respectively.

Figure 7 shows the continuous spectral profile of the object measured over the observation plane. This spectral profile is acquired from the volume interferogram obtained in this experiment. Three spectral peaks are located near 448 nm, 504 nm, and 630 nm. These peaks agree with the peak wavelengths of the measured objects. The phase distributions of the cross-spectral density at the three spectral peaks are shown in Fig 8. These phase distributions are essentially equivalent to the complex incoherent hologram for the corresponding spectral component of the object.

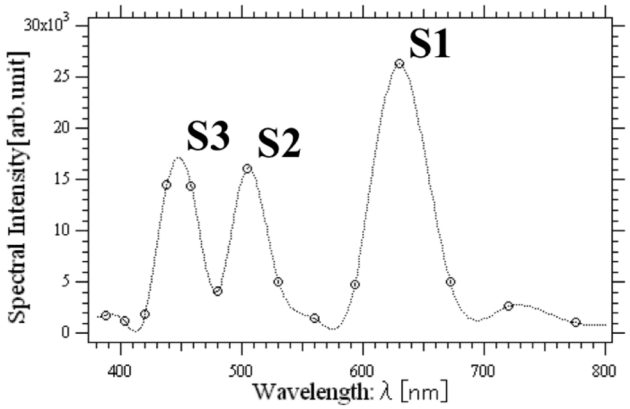

Fig 7. Continuous spectral profile of each light source: S1, S2 and S3.

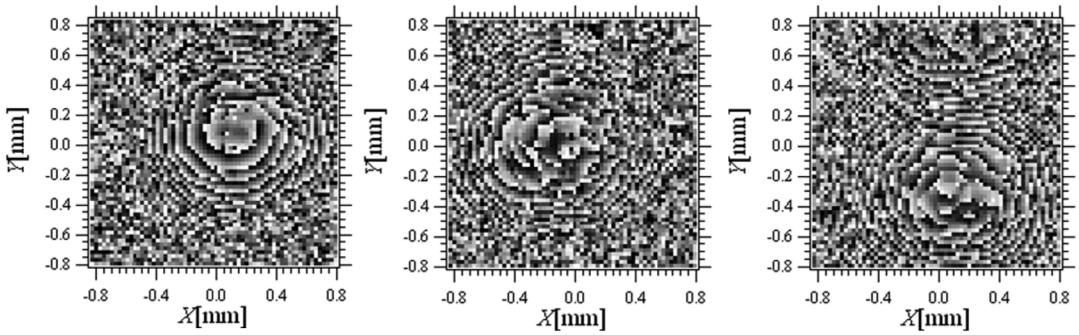

Fig 8. Phase distributions of cross-spectral densities at the each spectral peak: λ = 448nm (left), λ = 504nm (center), and λ = 630nm (right).

Finally, Fig 9 partly shows a whole set of the retrieved in-focus images for many spectral bands. Variation of intensity across the images agrees well with the retrieved spectral profile shown in Fig 7. We also find that the size of these images agree well with the actual size of the original light sources. As a result, a set of spectral components of 3D images of three planar light sources with different shapes of cross sections are successfully retrieved by digital holographic 3D imaging spectrometry.

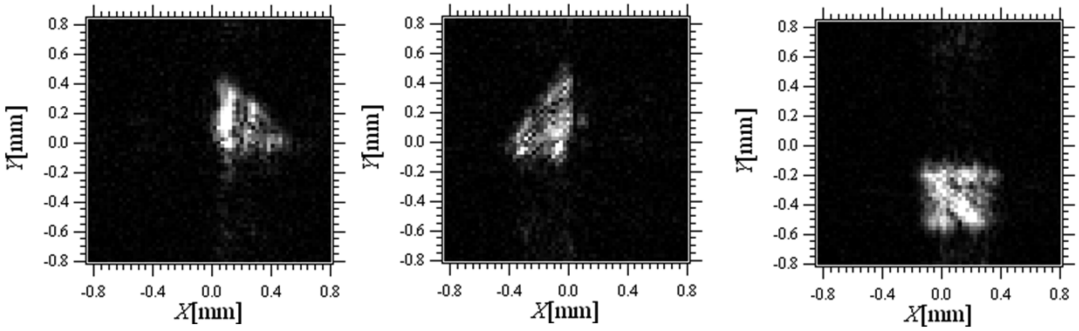

Fig 9. Retrieved in-focus image from each phase distribution over *x*-*y* plane at *z* = 70 mm (left), *z* = 61 mm (center), and *z* = 50 mm (right).

4 Conclusion

We have explained the method of the Fourier-transform spectral imaging technique and then introduced briefly the current status of this technique. The spectral image has been mainly used in the fields of astronomy and remote sensing. In the future, it is quite likely that the technique be developed in the fields closer to the people's daily life. We also expect that the further research might open the new field of applications of the spectral images.

References

1. Michelson A A, F. G. Pease, *Proc Natl Acad Sci* (*USA*), 7(1921)143-146.
2. Mertz L, Transformations in Optics, Secs. 3-4, (John Wiley & Sons, Inc., New York), 1965.
3. (a) Born M, Wolf E, Principles of Optics, Chap. 10, 4th edn, (Pergamon, London), 1970,
   (b) Mandel L, Wolf E, Optical Coherence and Quantum Optics, Sec. 4.4.4. ,(Cambridge University Press, Cambridge) 1995.
4. Fomalont E B, *Proc IEEE*, 61(1973)1211-1218.
5. Michelson A A, *Phil Mag Ser* 5, 31(1891)338-346.
6. Wolf E, Carter W H, *J Opt Soc Am*, 68(1978)953-964.
7. Itoh K, Ohtsuka Y, *J Opt Soc Am A*, 3(1986)94-100.
8. Mariotti J M, Ridgway S T, *Astron Astrophys*, 195(1988)350-363.
9. Shaklan S B, Roddier F, *Appl Opt*, 26(1987)2159-2163.
10. Mariotti J M, Coudé du Foresto V, Perrin G, Zhao P, Léna P, *Astron Astrophys,Suppl Ser*, 116(1996)381-393.
11. Ohta I S, Hattori M, Matsuo H, *Appl Opt*, 45(2006)2576-2585.
12. Ohta I S, Hattori M, Matsuo H, *Appl Opt*, 46(2007)2881-2892.
13. Moran J M, *Proc IEEE*, 61(1973)1236-1242.
14. Clark B G, *Proc IEEE*, 61(1973)1242-1248.
15. Bos A, Raimond E, van Someren Greve H W, *Astron Astrophys*, 98(1981)251-259.
16. Swenson G W, *J Opt Soc Am A*, 3(1986)1311-1319.
17. Marsh K A, Hurford G J, *Ann Rev Astron Astrophys*, 20(1982)497-516.
18. Chikada Y, Ishiguro M, Hirabayashi H, Morimoto M, Morita K, Kanzawa T, Iwashita, Nakazima K, Ishikawa S, Takahashi T, Handa K, Kasuga T, Okumura S, Miyazawa T, Nakazuru T, Miura, Nagasawa S, *Proc IEEE*, 75(1987)1203-1210.
19. Leisawitz D. Baker C. Barger A, Benford D, Blain A , Rob Boyle, Richard Broderick, Jason Budinoff, John Carpenter, Richard Caverly, Chen P, Cooley S, Christine Cottingham, Julie Crooke, Dave DiPietro, Mike DiPirro, Michael Femiano, Ferrer A, Jacqueline Fischer, Gardner J P, Hallock L, Harris K, Hartman K, Martin Harwit, Lynne Hillenbrand, Hyde T, Drew Jones, Jim Kellogg, Alan Kogut, Marc Kuchner, Bill Lawson, Javier Lecha, Maria Lecha, Amy Mainzer, Jim Mannion, Anthony Martino, Paul Mason, John Mather, Gibran McDonald, Rick Mills, Lee Mundy, Stan Ollendorf, Joe Pellicciotti, Dave Quinn, Kirk Rhee, Stephen Rinehart, Tim Sauerwine, Robert Silverberg, Terry Smith, Gordon Stacey, Stahl H P, Staguhn J, Tompkins S, Tveekrem J, Wall S, Wilson M, *Advances in Space Research*, 40 (2007)689-703.
20. Rinehart S A, Leisawitz D T, Bolcar M R, Chaprnka K M, Lyon R G, Maher S F, Memarsadeghi N, Sinukoff E J, Teichman E, *Proc SPIE*, 7734(2010)77342D-1; doi:10.1117/12.857108
21. Rizzo M J, Mundy L G, Dhabal A, Fixsen D J, Rinehart S A, Benford D J, Leisawitz D, Silverberg R, Veach T, Juanola-Parramon R, *Publications of the Astronomical Society of the Pacific*, 127(2015)1045-1060.
22. Marks D L, Stack R A, Brady D J, Munson D C, Brady R B, *Science*, 284(1999)2164-2166.
23. Rosen J, Brooker G, *Opt Lett*, 32(2007)912-914.
24. Rosen J, Brooker G, *Opt Express*, 15(2007)2244-2250.

25. Kim M K, *Opt Express*, 21(2013)9636-9642.
26. Naik D N, Pedrini G, Takeda M, Osten W, *Opt Lett*, 39(2014)1857-1860.
27. Itoh K, in Progress in Optics XXXV, ed E Wolf, (North-Holland, Amsterdam), 1996, pp.145.
28. Rizzo M J, Rinehart S A, Barry R K, Benford D J, Fixsen D J, Kale T, Leisawitz D T, Lyon R G, Mentzell E, Mundy L G, Silverberg R F, *Proc SPIE*, 8445(2012)84451T-1; doi:10.1117/12.925593
29. Leisawitz D, Bolcar M R, Lyon R G, Maher S F, Memarsadeghi N, Rinehart S A, Sinukoff E J, *Proc SPIE*, 8445(2012)84450A-1; doi:10.1117/12.926812
30. Yoshimori K, *J Opt Soc Am A*, 18(2001)765-770.
31. Sasamoto M, Yoshimori K, *Opt Rev*, 19(2013)29-33.
32. Teeranutranont S, Yoshimori K, *Appl Opt*, 52(2013)A388-A396.
33. Hashimoto T, Hirai A, Yoshimori K, *Appl Opt*, 52(2013)1497-1504.
34. Obara M, Yoshimori K, *Opt Rev*, 21(2014)479-485.

[Received: 1.11.2015]

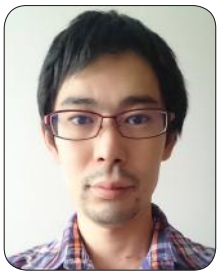

Masaki Obara received his BE and ME degrees in Computer Science from Iwate University, Iwate, Japan, in 2007 and 2009, respectively, and a PhD degree in Engineering from Iwate University in 2014. He is currently Research Associate at Iwate University from 2014. His research interests are digital holography, incoherent holography, multi-spectral imaging, and interferometric 3D imaging. He is a member of the Optical Society of Japan (OSJ) and the Japan Society of Applied Physics (JSAP).

Kyu Yoshimori received his BE, ME, and PhD degrees in applied physics from Osaka University, Osaka, Japan, in 1981, 1983, and 1994, respectively. He is now an associate professor in the Department of Systems Innovation Engineering, faculty of Science and Engineering, Iwate University. He worked for Furuno Electric Co., Ltd. and National Space Development Agency of Japan in 1983-1997 and 1997-2000, respectively. His research interests are in the field of information photonics with emphasis on incoherent holography. He is also interested in the field of coherence and statistical optics, optical sensing, and optical metrology. He is a member of the Optical Society of America (OSA), the International Society for Optical Engineering (SPIE), the Japan Society of Applied Physics (JSAP), and the Optical Society of Japan (OSJ).

Kazuyoshi Itoh received his BE and ME degrees in applied physics from Osaka University, Osaka, Japan, in 1971 and 1975, respectively, and his PhD degree from Hokkaido University, Hokkaido, Japan, in 1984. He is now a Professor Emeritus and Research Professor of Osaka University. He worked for Nippon Kokan K. K. and Matsushita Electric Industrial Co., Ltd. in 1971-1972 and 1975-1978, respectively. Since 1978, he worked for Hokkaido University and moved to Osaka University in 1986. Since 1995, he was a Professor of Osaka University until March of 2013. He is presently a Board Member of Neubrex Co. Ltd., a start-up company from Osaka University. He is interested in applications of coherence theory and ultra-short optical

pulses to optical signal processing, material processing, and bio-photonics in recent years. He served as the Editor-in-Chief of the Japanese Journal of Optics in 1997-1999 and the Editor-in-Chief of Japanese Journal of Applied Physics in 2003-2004 and the President of the Optical Society of Japan in 2006-2008. He is a Fellow of the Optical Society of America (OSA), the International Society for Optical Engineering (SPIE), the Japan Society of Applied Physics (JSAP). He is the recipient of the 2015 Dennis Gabor award of the SPIE.